Appl Phys B (2011) 105:203–211
DOI 10.1007/s00340-011-4725-7

Applied Physics B
Lasers and Optics

Stimulated Raman rotational photoacoustic spectroscopy using a quartz tuning fork and femtosecond excitation

W. Schippers · E. Gershnabel · J. Burgmeier · O. Katz · U. Willer · I.S. Averbukh · Y. Silberberg · W. Schade

Received: 31 May 2011 / Revised version: 1 August 2011 / Published online: 11 September 2011

Abstract Molecular alignment of linear molecules (O_2, N_2, CO_2 and CO) is measured photoacoustically in the gas phase. The rotational excitation is accomplished using a simple femtosecond stimulated Raman excitation scheme, employing two femtosecond pulses with variable delay between the pulses. Molecular alignment is determined directly by measuring the energy dumped into the gas by quartz-enhanced photoacoustic spectroscopy (QEPAS), utilizing a quartz tuning fork as a sensitive photoacoustic transducer. The experimental results demonstrate for the first time the use of a tuning fork for resonant photoacoustic detection of Raman spectra excited by femtosecond double pulses and match both simulation and literature values.

1 Introduction

In recent years, several authors reported measurements of revivals in molecular alignment experiments performed with gases like nitrogen and oxygen. The majority of the experiments reported used birefringence effects to measure molecular alignment [1] or relied on intense Coulomb explosion pulses and subsequent measurement of the orientation of the resulting molecular fragments [2]. Another approach uses the fact that the ionization probability and high harmonic generation yield depend on the alignment of the molecules [3].

In this paper, we report a simple method to measure the alignment-dependent energy dumped into gaseous linear molecules by quartz-enhanced photoacoustic spectroscopy (QEPAS [4]). Our technique is based on molecular alignment by stimulated Raman double-pulse excitation using femtosecond (fs) pulses, and acoustic detection of the dumped energy using a high-Q piezoelectric tuning fork. Numerous techniques have been suggested recently for laser molecular alignment, which use single or multiple short laser pulses (transform limited or shaped) to temporarily align molecular axes along certain directions (for an introduction to the rich physics of laser molecular alignment, see e.g. [5–13]). Short laser pulses excite rotational wavepackets, which results in a considerable transient molecular alignment after the laser pulse is over, i.e. at field-free conditions. Traditional methods for measuring laser-induced molecular alignment are usually based on ultra-fast measurements of molecular angular distribution or related changes in the optical properties of the excited molecular medium.

Our experimental apparatus contains only an interferometer for generating the double excitation pulses of equal intensity and a gas cell with a quartz tuning fork microphone. The alignment of the molecules is quantified directly by measuring the amount of dumped light energy converted to heat, and consequently results in pressure change and acoustic signal.

W. Schippers · J. Burgmeier · U. Willer · W. Schade (✉)
Clausthal University of Technology, Energy Campus/EFZN, Am Stollen 19, 38640 Goslar, Germany
e-mail: wolfgang.schade@tu-clausthal.de
Fax: +49-5321-6855159

E. Gershnabel · I.S. Averbukh
Department of Chemical Physics, The Weizmann Institute of Science, Rehovot 76100, Israel

O. Katz · Y. Silberberg
Department of Physics of Complex Systems, The Weizmann Institute of Science, Rehovot 76100, Israel

W. Schade
Fraunhofer Heinrich Hertz Institute, Energy Campus, Am Stollen 19, 38640 Goslar, Germany

One of the major advantages of using photoacoustic detection for Raman spectroscopy is that it measures directly the amount of energy dumped into the molecules by the Raman process. This is in contrast to conventional Raman spectroscopy where the weak signal originates from the Raman-shifted (anti-Stokes or Stokes) photons; this requires high-quality optical filtering to separate the Raman-shifted photons from the pump photons and sensitive optical detectors. These merits make photoacoustics an ideal background-free technique for measuring rotational spectra with small Raman shifts [14]. Indeed, there have been a few photoacoustic Raman spectroscopy (PARS) experiments using conventional microphones at audio frequencies [15, 16]. However, the use of conventional audio-band microphones suffers from high sensitivity to the environmental background noise and structural vibrations. The use of high-Q quartz tuning forks instead of conventional microphones minimizes the influence of ambient noise for three reasons: first, the relatively high resonance frequency of the detector (∼32.7 kHz) is far off the ambient noise range (usually below 500 Hz). Second, the high quality factor of approximately $Q = 10\,000$ of the detector itself enhances the signal to noise (S/N) ratio of the system. Last, the piezoelectric tuning fork generates an electric signal if both of its prongs bend in opposite directions. Therefore, ambient sound energy originating from sources which are far from the detector do not effectively excite such specific oscillations.

2 Rotational Raman processes induced by fs double pulses

A linearly polarized femtosecond pulse interacting with a polarizable molecule without a permanent dipole moment induces a temporal dipole moment in it and subsequently exerts a torque on the molecule, therefore inducing molecular rotations. Because of the laser pulses being considerably shorter than the molecular rotational periods, most of the rotational dynamics happens after the electric field of the laser pulse faded out. Under these field-free conditions, the molecules continue to rotate and form a so-called rotational wavepacket. This wavepacket takes the most aligned shape shortly after the end of the pulse; afterwards, the temporal alignment vanishes due to the wavepacket dispersion. However, after one rotational revival period T_{rev} (or integer multiples of it) the molecule's alignment distribution that existed immediately after the first pulse is restored. This happens because of the constructive quantum interference of the discrete rotational energy states forming the wavepacket. After the revival, the temporal evolution of the wavepacket repeats once again. Fractional revivals are observed at $T_{\mathrm{rev}}/4$, $T_{\mathrm{rev}}/2$ and $3T_{\mathrm{rev}}/4$. Rotational revivals are manifestations of the general phenomenon of the revivals of quantum wavepackets, which was observed in multiple atomic, molecular and quantum optical systems [17, 18].

The rotational revival period T_{rev} of linear molecules is given by

$$T_{\mathrm{rev}} = \frac{1}{2Bc}, \tag{1}$$

where $B = h/(8\pi^2 Ic)$ is the molecular rotational constant in cm^{-1} (I is the moment of inertia of the respective molecule).

As explained above, the alignment of the molecules changes periodically after a single laser pulse is applied. When a double-pulse scheme is used, the impact of the second laser pulse depends on the time delay between the two pulses. The rotation of the molecules that was induced by the first pulse can be slowed down or accelerated by the second short pulse depending on the angle between laser polarization and the position of the molecular axis at the incidence of the second pulse. With elapsing time, the rotational (R) energy is converted into translational (T) energy via R–T-transfer processes, resulting in an increased temperature. The more rotational excitation is provided by the pulse pair, the more energy is converted into translations, which in turn is directly measurable as temperature/pressure changes by the acoustic transducer.

3 Experimental setup

3.1 Generation of double pulses

The experimental setup (Fig. 1) consists of a femtosecond laser (Coherent Mantis, $f = 80$ MHz, $P = 500$ mW) seeding a regenerative amplifier (Spectra Physics, Spitfire Pro-35). The amplifier emits pulses at $\lambda = 800$ nm with a bandwidth of $\Delta\lambda = 45$ nm. Pulse durations used in these experiments were about $\tau = 50$ fs. The amplifier can be triggered externally to emit pulses with repetition rate between 8 kHz and 12 kHz. The amplified pulses enter an interferometer setup: the pulse is split into two identical replicas, with a computer-controlled time delay of up to 50 picoseconds (ps). The two pulses are recombined to a single beam by use of a second beam splitter. The double-pulse laser beam is focused by an $f = 100$ mm lens into a gas cell. The gas cell features two 2-mm-thick BK7 windows with an antireflection coating at the beam's entrance and exit. An iris diaphragm with approximately $d = 5$ mm diameter is placed before the cell to prevent stray radiation in the cell.

To estimate the power density in the focal spot, a beam radius of roughly 2.5 mm can be assumed. The focal area after the lens can be calculated to be approximately $A = 3.3 \times 10^{-6}$ cm^2. A typical average power used for the measurements is $P = 100$ mW, so the pulse energy is $E_{\mathrm{p}} =$

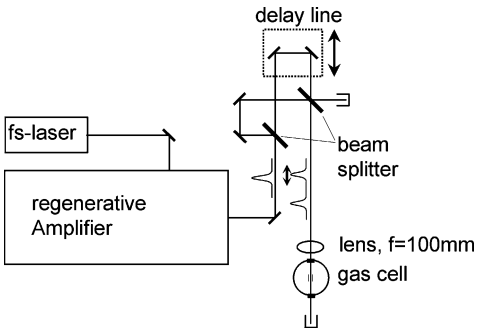

Fig. 1 Setup of the double-pulse experiment

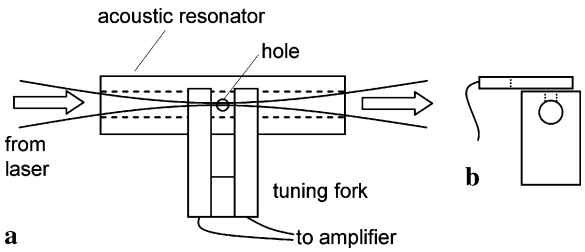

Fig. 2 Tuning fork in off-beam configuration. (**a**) Viewed from above, (**b**) front view of the resonator in beam direction

100 mW/10.9 kHz = 9.17 µJ. With a pulse duration $\tau =$ 50 fs, a peak power $P_{\text{peak}} = E_{\text{p}}/\tau = 183$ MW can be derived. Therefore, the power density at the focus is approximately $I_{\text{peak}} = P_{\text{peak}}/A = 5.6 \times 10^{13}$ W/cm^2.

3.2 Photoacoustic QEPAS detector

For the detection of the rotational energy dumped into the molecules, photoacoustic spectroscopy is applied by use of a quartz tuning fork as transducer. The excitation of molecules for QEPAS is commonly done by spectrally tuning a modulated laser beam to a strong absorption line of the molecules under investigation. The molecules then relax via vibrational–translational transfer processes and the energy is present in the form of a sound wave which can be detected with the tuning fork because bending of the prongs gives rise to a piezo current. The same sensing principle is used in this experiment except for the excitation process, which is in this case a nonlinear impulsive Raman (two-photon) excitation.

Figure 2 shows the tuning fork detector within the gas cell (inner diameter: 80 mm) positioned 8 mm behind the entrance window. It consists of the tuning fork itself and an acoustic resonator which is aligned in off-beam configuration [19]. The laser beam is focused through a 5.8-mm-long hole of $d = 0.8$ mm diameter within a brass block (1.5 mm × 4.0 mm × 5.8 mm) acting as an acoustic resonator. The optimal resonator length was chosen according to Ref. [19]. Within the resonator, energy is dumped into the molecules depending on the temporal separation of the two pulses. As a result, an acoustic standing wave is formed, with a pressure maximum located at the center of the open-ended resonator. A hole directly above the resonator's center directs the pressure wave between the prongs of a commercially available dismantled tuning fork used for quartz watches ($f_{\text{res.}} = 32.768$ kHz, dimensions of both prongs: 4.5 mm × 1.5 mm × 0.31 mm) as shown in Fig. 2b. The tuning fork is positioned as near to the brass block as possible (gap ≈ 0.1 mm); the thickness of the resonator wall at this upper side is 0.3 mm. The prongs are driven by the pressure waves which exhibit the same repetition frequency as the laser. The piezo current induced by the prongs' bending is amplified by a home-made transimpedance amplifier (with a gain of 10^7 V/A) and is measured by a lock-in-amplifier.

In order to effectively excite the tuning fork, it is crucial to exactly adjust the laser's repetition rate to the tuning fork's resonance frequency or an integer divisor of it. Given the maximum repetition rate achievable by the Spitfire-Pro regenerative amplifier of 12 kHz, we chose the highest applicable laser repetition rate, which is approximately 32.7 kHz/3 = 10.9 kHz. At this pulse repetition rate the excited tuning fork oscillates at the 3rd harmonic of the repetition rate. The lock-in amplifier reference frequency is set as well by the amplifier frequency generator and lock-in measurements are performed at the 3rd harmonic. The exact resonance frequency of the tuning fork is dependent on the gas type and gas pressure in the cell and has to be redetermined each time the ambient conditions are changed. The temperature dependency of the tuning fork's resonance frequency is negligible at normal laboratory conditions as the cut angle of the quartz crystal is already specifically chosen for commercially available tuning forks (temperature dependence of resonance frequency in the order of 10^{-6} K^{-1} [20]). The system's (tuning fork + acoustic resonator) Q-factor has been measured to be around $Q = 9500$ at ambient pressure.

In our setup, the use of a lock-in-amplifier and measurement at higher harmonics further enhances the signal to noise ratio by suppressing pickup of electrical stray radiation generated by controllers of the laser system, in particular by high-voltage peaks used for the Pockels cells of the femtosecond amplifier.

3.3 Measurement procedure

Prior to the measurements, the gas cell is evacuated with a rotary vane pump and filled to room pressure with the gas to measure. The laser's repetition rate is adjusted to the tuning fork's resonance frequency by maximizing the lock-in-signal while blocking one arm of the interferometer to prevent any specific excitation of the gas molecules; the absorption of the single laser pulses is sufficient for this task. After that, both interferometer arms are unblocked and the zero-delay position of the delay stage is determined by using the double-pulse setup as an autocorrelator.

To measure the rotational spectra, the delay between the pulses is repeatedly increased by a small amount (typically by increments of 1.2 µm optical path length, i.e. a relative delay of 4 fs) and the respective lock-in-signals are recorded. With this procedure, time-dependent traces are acquired which give the tuning fork signal (i.e. the photoacoustic signal, which is proportional to the amount of energy dumped into the gas molecules) as a function of the temporal pulse separation of the femtosecond double pulses.

4 Simulation

Our measurements for a selection of different molecules resulted in a rich variety of time-dependent signals exhibiting periodic sequences of peaks of different shapes. To sort through the accumulated data, a simulation of the time-dependent dynamics of the process was carried out following the procedure detailed in Appendix. These simulations resulted in graphs showing the dependences of the angular distribution and dumped energy on the temporal delay between the two laser pulses interacting with the molecules. Within the adopted model of a rigid rotor, the position of the peaks is determined by T_{rev} (and its fractions). The shape of the peaks and their magnitudes depend on the dimensionless kick strength of the laser pulses $P_{1,2}$, the dimensionless temperature of the gas $\sigma_{\mathrm{th}} = (k_{\mathrm{B}}T/2B)^{1/2}$ and the symmetry of the molecules (refer to Appendix). In the simulations, laser pulses of kick strengths $P_{1,2} = 10$ were considered, which is a representative value for the laser intensity used as well as the polarizability range of the molecules measured, and $\sigma_{\mathrm{th}} = 7.24$, which corresponds to $T = 300$ K for nitrogen molecules.

While calculating the ensemble averaging, the symmetry of the molecule and the associated wavefunction, and the spin properties of the nuclei have to be taken into account, leading to certain J-state selection rules. In the case of oxygen, only odd J states are relevant. For CO_2, one expects only even J states being occupied. The spectra of carbon monoxide molecules show contributions from both even and odd J states. Finally, a ratio of even:odd = 2:1 is expected for the spin-statistical factors for $^{14}N_2$. For the isotope $^{15}N_2$, the corresponding ratio of even:odd = 1:3 can be expected. A $^{14}N^{15}N$ molecule features both even and odd J states in equal proportions [21]. Since most of the natural nitrogen consists of the $^{14}N_2$ isotope, a ratio between even and odd J states being 2:1 was assumed [22].

5 Comparing simulation to experimental results

5.1 Results for odd J states

In Fig. 3a and b, the thermal averages of alignment and excitation energy for odd J states of the ensemble are given. In the upper graph the alignment after the first pulse is plotted versus the time after the first pulse. In Fig. 3b, the energy after the second pulse is plotted versus the delay between the two pulses, given in units of T_{rev}. When considering these two graphs together, one gets a clear understanding of the measured signal patterns in Fig. 3c. When the average molecular alignment induced by the first pulse is rising (molecular axes are moving towards the polarization direction of the first pulse), the second pulse enhances molecular rotation and adds to the energy deposited in rotations. On the contrary, when the alignment is decreasing, the second pulse applies a torque working against the molecular rotation, and it reduces the rotational energy. If the second pulse is applied at the moment of the maximal alignment, the torque produced by the second pulse is minimal, and it practically does not alter the rotational energy.

It follows from Fig. 3a and b that with only odd J states being excited, one should observe revivals of the photoacoustic signal at every integer multiple of $T_{\mathrm{rev}}/4$. This is consistent with the general scenario of fractional revivals [17]. The odd and even J states contribute to revivals at integer multiples of $T_{\mathrm{rev}}/4$ with opposite signs about the background alignment. In case of equal statistical weights of the even and odd J states, these peaks coherently cancel each other. Different statistical weights for the odd and even J states, however, result in the residual alignment peaks at these positions in time.

The excitation energy graph can be compared with the experimental results, since the photoacoustic signal is directly correlated with the amount of rotational energy dumped into the molecules. As explained above, for oxygen only odd J states should be occupied. Varying the temporal pulse spacing of the femtosecond double pulses and measuring the associated photoacoustic signal by the tuning fork sensor inside an oxygen-filled cell results in the diagram shown in Fig. 3c. For oxygen, the rotational constant is $B = 1.4376\ \mathrm{cm}^{-1}$ [23], so the expected revival time is around $T_{\mathrm{rev}} = 11.6$ ps, which results in the signal revival after every $T_{\mathrm{rev}}/4 = 2.9$ ps. When compared to the result of the simulation for odd J in Fig. 3b, the relative intensities of the different measured features are a bit off compared to the simulation, but with respect to the temporal characteristics of the peaks and dips the graphs look alike. Analyzing the measured data by determining the temporal distances between the features in Fig. 3c (experimental data up to 50 ps of time between pulses has been used for better accuracy) results in an experimental rotational constant of $B = (1.435 \pm 0.003)\ \mathrm{cm}^{-1}$, which is in good agreement to the above-mentioned literature value.

5.2 Results for even J states

Figure 4 shows the simulation results for even J states of the N_2 ensemble. Like in the odd J case, we expect revivals at

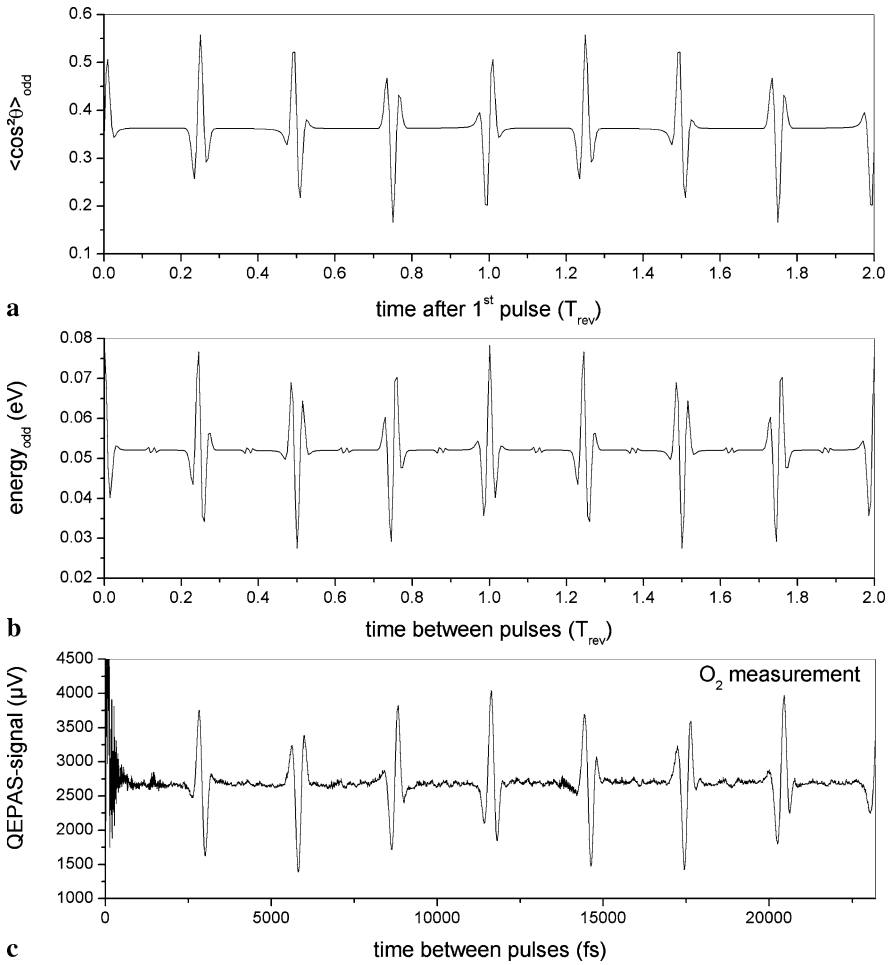

Fig. 3 Simulation results for odd J states. (**a**) Time dependency of molecule alignment after one laser pulse, (**b**) energy stored in molecules after two pulses dependent on the pulse delay, (**c**) measured pulse delay dependent photoacoustic signal for oxygen

every integer multiple of $T_{\mathrm{rev}}/4$, but this time the characteristics of the signal are different from those shown in Fig. 3. For example, for even J states the first peak at $T_{\mathrm{rev}}/4$ shows mainly a decrease in the rotational energy instead of an increase as derived for the odd J case.

CO_2 may be considered [24] as an example of molecules with only even J states occupied. The rotational constant is $B = 0.3902\ \mathrm{cm}^{-1}$ ([25], p. 396) and therefore the revival time is 42.7 ps. Experimental results for CO_2 are shown in Fig. 4c. All measurements shown in this paper were done with a temporal delay up to 50000 fs; therefore, the CO_2 graphs do not reach $2T_{\mathrm{rev}}$, contrary to the others. The positions of the peaks are in good agreement with the simulation, and the measured rotational constant $B = (0.390 \pm 0.001)\ \mathrm{cm}^{-1}$ coincides with the literature value. However, it appears that the temporal behavior of the CO_2 experimental results is inverted compared to the simulation (see Fig. 4b). For delay times that result in an increase of dumped energy, a decrease is measured in the acoustic signal and vice versa. Evidently, the presented measurements for CO_2 are not reproduced by the adopted simple model involving only rotational excitation by double pulses. Possible reasons for this are discussed at the end of the paper.

5.3 Results for even and odd J states

5.3.1 Evenly distributed mixture

The simulations shown in Fig. 5 are for an ensemble that contains both even and odd J states with the same statistical weight. The reason that the corresponding graphs look rather flat at quarter revivals and only have peaks at the half revivals and full revivals is due to the destructive and constructive interference of the two contributions from the even and odd J states [22].

For carbon monoxide featuring both even and odd J states, the rotational constant is $B = 1.9226\ \mathrm{cm}^{-1}$ [26], so the revival time is approximately $T_{\mathrm{rev}} = 8.7$ ps. In the experiment (Fig. 5c), we observe the same structure as predicted by theory: revivals at odd multiples of $T_{\mathrm{rev}}/4$ are completely suppressed, and only the ones at multiples of $T_{\mathrm{rev}}/2$ remain; refer e.g. to $T_{\mathrm{rev}}/2 = 4.3$ ps. Calculating the rotational constant out of the measured data results in $B = (1.919 \pm 0.004)\ \mathrm{cm}^{-1}$.

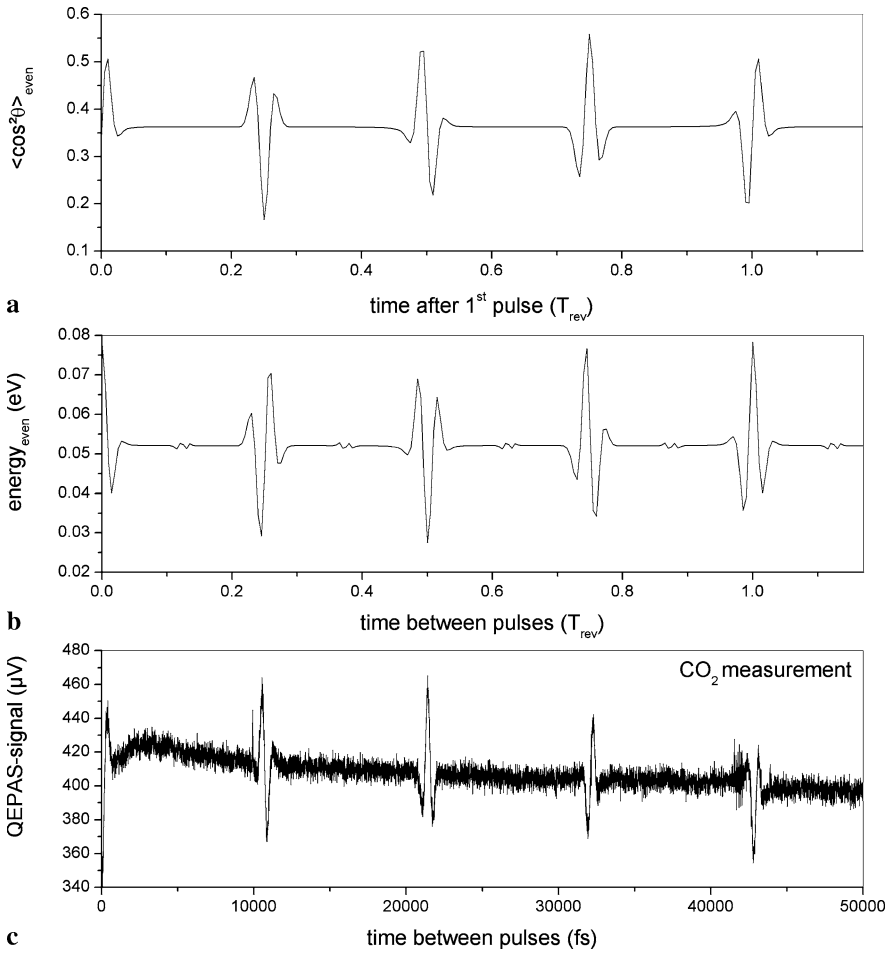

Fig. 4 Simulation results for even J states. (**a**) Time dependency of molecule alignment after one laser pulse, (**b**) energy stored in molecules after two pulses dependent on the pulse delay, (**c**) measured pulse delay dependent photoacoustic signal for carbon dioxide

5.3.2 2:1 mixture of even and odd J states

As described above, for natural nitrogen one expects a ratio of 2:1 for the spin-statistical factors for even and odd J states, respectively. As shown in Fig. 6, the simulation results in this case in weak revivals at odd multiples of $T_{\mathrm{rev}}/4$ and strong revivals at multiples of $T_{\mathrm{rev}}/2$. So, contrary to Fig. 5 (even and odd states being equally represented), the revivals at odd multiples of $T_{\mathrm{rev}}/4$ are not fully suppressed.

Measuring the photoacoustic signal of femtosecond double pulses of variable delay inside a nitrogen-filled gas cell (Fig. 6c), one expects a rotational constant $B = 1.9896\ \mathrm{cm}^{-1}$ [21] and therefore a revival time of approximately 8.4 ps, which matches both experimental and simulation results as well as the experimentally acquired rotational constant $B = (1.987 \pm 0.003)\ \mathrm{cm}^{-1}$.

6 Discussion

The presented experimental setup allows the photoacoustic measurement of double pulse induced alignment of gas molecules using a quartz tuning fork as a detector. The experimental results agree well with theoretical simulations for different combinations of even and odd J states. The only exception is the carbon dioxide measurements, which differ as the measured signal shows an inverted behavior in the increase and decrease of the dumped energy.

An intensity of $5.6 \times 10^{13}\ \mathrm{W/cm^2}$ resulted in the best signal to noise ratio for all measurements. When using more power, an irregular noise background appeared in the graphs and tended to mask the alignment peaks. This is in line with other molecular alignment experiments [27, 28] and the intensities used are well below the ionization threshold of $2 \times 10^{14}\ \mathrm{W/cm^2}$ for N_2 [29]. According to this, in most of the presented experiments the molecules should be aligned, but not ionized. However, as CO_2 exhibits a significantly higher polarizability anisotropy $\Delta\alpha$ [30], the kick strength $P \sim \Delta\alpha$ resulting from the same laser intensity is much higher. Furthermore, for CO_2 the applied laser intensity is near the ionization threshold (slightly below $8 \times 10^{13}\ \mathrm{W/cm^2}$ [31]); therefore, complex multi-photon processes may occur, such as ionization, which is also alignment dependent [3, 29, 32]. This may influence the energy

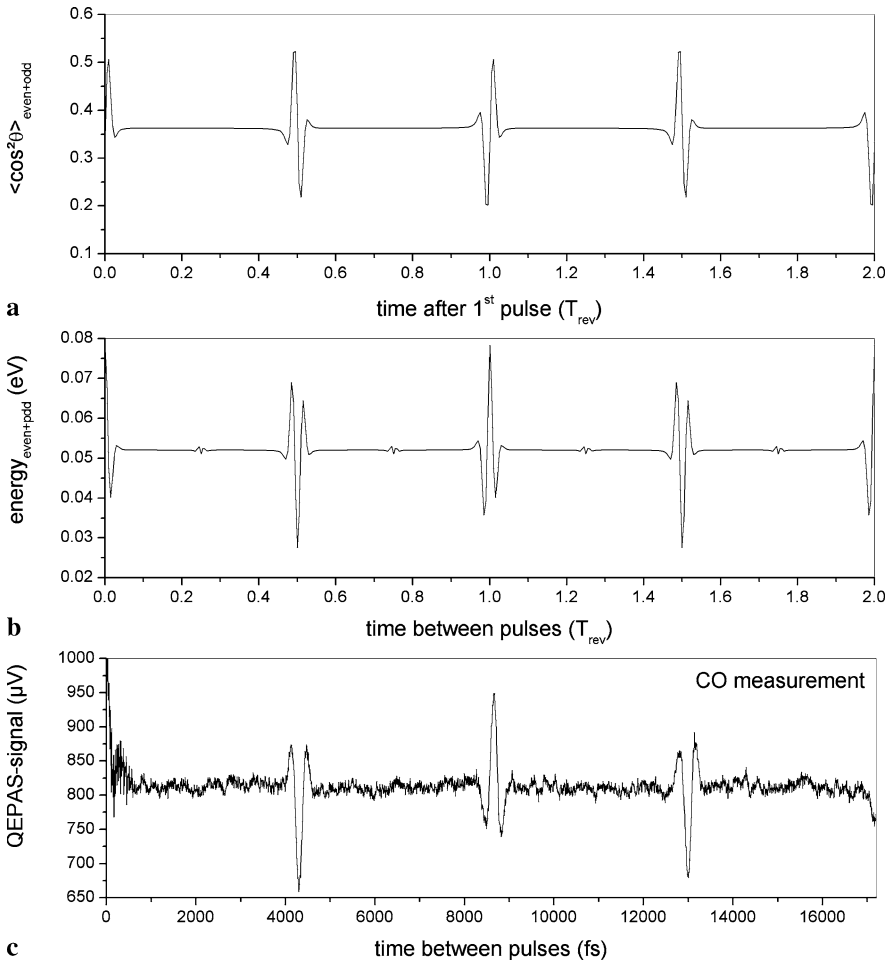

Fig. 5 Simulation results for even + odd J states. (**a**) Time dependency of molecule alignment after one laser pulse, (**b**) energy stored in molecules after two pulses dependent on the pulse delay, (**c**) measured pulse delay dependent photoacoustic signal for carbon monoxide

balance in generating the acoustic signal and explain the deviations from the simple simulation model adopted in this paper.

Following investigations will concentrate on the effect of the pulse width, pulse intensity and polarization of the respective pulses and the use of schemes with more than two pulses. In general, the shown detection setup may not only be used for a rough determination of rotational constants, but also as an alternative photoacoustic detection approach useful in e.g. femtosecond pulse shaping setups for the detection of more complicated molecules.

Acknowledgements This work was supported in part by the German Federal Ministry of Education and Research, contract number 13N9475, and by NATO, project number SfP-983789. We appreciate discussions with Uri Steinitz. Erez Gershnabel and Ilya Sh. Averbukh acknowledge the support by a grant from the Israel Science Foundation.

Appendix: Simulation procedure

The Hamiltonian of a linear molecule interacting with a non-resonant laser field is given by

$$\hat{H} = \frac{\hat{J}^2}{2I} + V(\theta, t), \tag{2}$$

where $\hat{J}$ is the angular momentum operator and V is the energy of interaction between the molecule and the laser field:

$$V(\theta, t) = -\frac{1}{4}\varepsilon^2(t)\left[\Delta\alpha \cos^2\theta + \alpha_\perp\right]. \tag{3}$$

Here ε is the laser electric field envelope and θ is the angle between the molecular axis and the polarization of the laser pulse. The polarizability anisotropy is given by $\Delta\alpha = \alpha_{||} - \alpha_\perp$, where $\alpha_{||}, \alpha_\perp$ are the parallel and perpendicular polarizability components of the molecule, respectively. If the laser pulse is short compared to the typical periods of molecular rotation, it may be considered as a delta pulse. In this impulsive approximation, one obtains the following

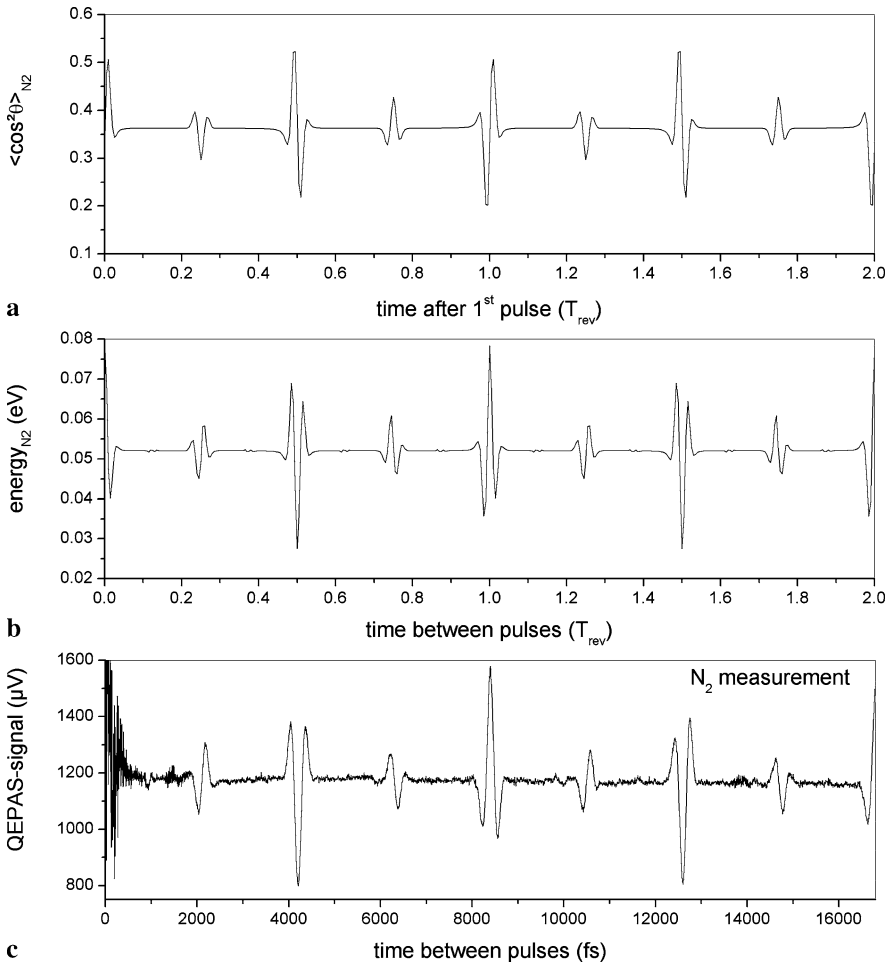

Fig. 6 Simulation results for an even:odd J states ratio of 2:1. (**a**) Time dependency of molecule alignment after one laser pulse, (**b**) energy stored in molecules after two pulses dependent on the pulse delay, (**c**) measured pulse delay dependent photoacoustic signal for nitrogen

relation between the angular wavefunctions immediately before and after the pulse applied at $t = 0$ (see e.g. [33]):

$$\psi(t = 0^+) = \exp\left(\mathrm{i}P\cos^2\theta\right)\psi(t = 0^-), \tag{4}$$

where the kick strength P is given by

$$P = \frac{\Delta\alpha}{4\hbar}\int_{-\infty}^{\infty}\varepsilon^2(t)\,\mathrm{d}t. \tag{5}$$

Physically, the dimensionless kick strength P equals the typical amount of angular momentum (in units of $\hbar$) supplied by the pulse to the molecule.

The wavefunction is expanded in the basis of the spherical harmonics $|J, m\rangle$ and, for the vertical polarization of the laser field (which is the case in our work), m is a conserved quantum number. This allows us to consider the excitation of the states with different initial m values separately. In order to find $\psi(t = 0^+)$ for any initial state, we introduce an artificial parameter ξ that will be assigned the value $\xi = 1$ at the end of the calculations and define

$$\psi_\xi = \exp\left[\left(\mathrm{i}P\cos^2\theta\right)\xi\right]\psi(t = 0^-) = \sum_J c_J(\xi)|J, m\rangle. \tag{6}$$

By differentiating both sides of (6) with respect to ξ, we obtain the following set of differential equations for the coefficients c_J:

$$\dot{c}_{J'} = \mathrm{i}P\sum_J c_J\langle J', m|\cos^2\theta|J, m\rangle, \tag{7}$$

where $\dot{c} = \mathrm{d}c/\mathrm{d}\xi$. The matrix elements in (7) can be found using recurrence relations for the spherical harmonics [34]. Since $\psi_{\xi=0} = \psi(t = 0^-)$ and $\psi_{\xi=1} = \psi(t = 0^+)$ (see (6)), we numerically solve this set of equations from $\xi = 0$ to $\xi = 1$, and find $\psi(t = 0^+)$.

In order to consider the effect of the field-free alignment at thermal conditions, we repeated this procedure for every initial $|J_0, m_0\rangle$ state.

We consider a dimensionless time τ, such that $t = \tau \cdot t_q$, where $t_q \equiv I/\hbar = T_{\mathrm{rev}}/2\pi$. Thus, the free evolution after the laser pulse gives the wavefunction at $\tau = \tau_1$, right before the second laser pulse:

$$\psi_{J_0}^{m_0}(\tau_1) = \sum_{J=0}^{\infty} c_J \exp\left[-\frac{\mathrm{i}}{2}J(J+1)\tau_1\right]|J, m_0\rangle, \tag{8}$$

where c_J are the coefficients (from (7)) of the wavepacket that was excited from the initial state $|J_0, m_0\rangle$.

At every moment of time, the alignment factor is given by

$$\langle \cos^2\theta \rangle = \sum_{J_0=0}^{\infty} P(J_0) \sum_{m_0=-J_0}^{J_0} A_{J_0}^{m_0}(\tau), \tag{9}$$

where

$$P(J_0) = \frac{1}{Q} \exp\left[-\frac{J_0(J_0+1)}{2\sigma_{\text{th}}^2} \right] \tag{10}$$

is the thermal distribution, Q is the rotational partition function and $\sigma_{\text{th}} = (k_{\text{B}} T/2B)^{1/2}$ (k_{B} is the Boltzmann constant). In (9),

$$A_{J_0}^{m_0}(\tau) = \langle \psi_{J_0}^{m_0}(\tau) | \cos^2(\theta) | \psi_{J_0}^{m_0}(\tau) \rangle \tag{11}$$

is the contribution to the alignment factor from the initial state $|J_0, m_0\rangle$.

The wavefunction after the second pulse, including the free evolution, is calculated in the same manner as above, by means of (4) and (8), respectively.

Finally, in order to calculate the energy after the second pulse as a function of the delay time τ between the pulses, one considers the following equation:

$$\langle E \rangle = \sum_{J_0=0}^{\infty} P(J_0) \sum_{m_0=-J_0}^{J_0} E_{J_0}^{m_0}(\tau), \tag{12}$$

where

$$E_{J_0}^{m_0}(\tau) = \langle \psi_{J_0}^{m_0}(\tau) | \frac{\hat{J}^2}{2I} | \psi_{J_0}^{m_0}(\tau) \rangle. \tag{13}$$

Here $\psi_{J_0}^{m_0}$ refers to the wavefunction immediately after the second pulse.

References

1. J.P. Cryan, P.H. Bucksbaum, R.N. Coffee, Phys. Rev. A **80**, 063412 (2009)
2. K.F. Lee, I.V. Litvinyuk, P.W. Dooley, M. Spanner, D.M. Villeneuve, P.B. Corkum, J. Phys. B, At. Mol. Opt. Phys. **37**, L43 (2004)
3. X. Zhao, X.M. Tong, C.D. Lin, Phys. Rev. A **67**, 043404 (2003)
4. A.A. Kosterev, Y.A. Bakhirkin, R.F. Curl, F.K. Tittel, Opt. Lett. **27**, 1902 (2002)
5. B. Friedrich, D. Herschbach, Phys. Rev. Lett. **74**, 4623 (1995)
6. B. Friedrich, D. Herschbach, J. Chem. Phys. **111**, 6157 (1999)
7. H. Stapelfeldt, T. Seideman, Rev. Mod. Phys. **75**, 543 (2003)
8. V. Kumarappan, S.S. Viftrup, L. Holmegaard, C.Z. Bisgaard, H. Stapelfeldt, Phys. Scr. **76**, C63 (2007)
9. J.G. Underwood, B.J. Sussman, A. Stolow, Phys. Rev. Lett. **94**, 143002 (2005)
10. K.F. Lee, D.M. Villeneuve, P.B. Corkum, A. Stolow, J.G. Underwood, Phys. Rev. Lett. **97**, 173001 (2006)
11. D. Daems, S. Guérin, E. Hertz, H.R. Jauslin, B. Lavorel, O. Faucher, Phys. Rev. Lett. **95**, 063005 (2005)
12. E. Hertz, A. Rouzée, S. Guérin, B. Lavorel, O. Faucher, Phys. Rev. A **75**, 031403(R) (2007)
13. S. Guérin, A. Rouzée, E. Hertz, Phys. Rev. A **77**, 041404(R) (2008)
14. G.A. West, Rev. Sci. Instrum. **54**, 797 (1983)
15. D.R. Siebert, G.A. West, J.J. Barrett, Appl. Opt. **19**, 53 (1980)
16. A. Melchior, I. Bar, S. Rosenwaks, J. Phys. Chem. A **102**, 7273 (1998)
17. I.Sh. Averbukh, N.F. Perelman, Phys. Lett. A **139**, 449 (1989)
18. R.W. Robinett, Phys. Rep. **392**, 1 (2004)
19. K. Liu, X. Guo, H. Yi, W. Chen, W. Zhang, X. Gao, Opt. Lett. **34**, 1594 (2009)
20. R. Bechmann, A.D. Ballato, T.J. Lukaszek, Proc. IRE **50**, 1812 (1962)
21. J. Bendtsen, J. Raman Spectrosc. **2**, 133 (1974)
22. S. Fleischer, I.Sh. Averbukh, Y. Prior, J. Phys. B, At. Mol. Opt. Phys. **41**, 074018 (2008)
23. W.H. Fletcher, J.S. Rayside, J. Raman Spectrosc. **2**, 3 (1974)
24. G.A. West, J.J. Barrett, Opt. Lett. **4**, 395 (1979)
25. G. Herzberg, *Molecular Spectra and Molecular Structure II* (Van Nostrand, New York, 1945), reprinted 1991 with corrections, pp. 16–20
26. I.G. Nolt, J.V. Radostitz, G. DiLonardo, K.M. Evenson, D.A. Jennings, K.R. Leopold, M.D. Vanek, L.R. Zink, A. Hinz, K.V. Chance, J. Mol. Spectrosc. **125**, 274 (1987)
27. N. Xu, C. Wu, Y. Gao, H. Jiang, H. Yang, Q. Gong, J. Phys. Chem. A **112**, 612 (2008)
28. N. Xu, C. Wu, J. Huang, Z. Wu, Q. Liang, H. Yang, Q. Gong, Opt. Express **14**, 4992 (2006)
29. I.V. Litvinyuk, K.F. Lee, P.W. Dooley, D.M. Rayner, D.M. Villeneuve, P.B. Corkum, Phys. Rev. Lett. **90**, 233003 (2003)
30. F. Baas, K.D. van den Hout, Physica **95A**, 597 (1979)
31. X. Liu, Y. Liu, H. Liu, Y. Deng, C. Wu, Q. Gong, J. Opt. Soc. Am. B **28**, 293 (2011)
32. D. Pavičić, K.F. Lee, D.M. Rayner, P.B. Corkum, D.N. Villeneuve, Phys. Rev. Lett. **98**, 243001 (2007)
33. E. Gershnabel, R.J. Gordon, I.S. Averbukh, Phys. Rev. A **73**, 061401(R) (2006)
34. G.B. Arfken, H.J. Weber, *Mathematical Methods for Physicists*, 6th edn. (Elsevier/Academic Press, San Diego, 2005)